



National Research Institute of Astronomy and Geophysics
NRIAG Journal of Astronomy and Geophysics

www.elsevier.com/locate/nrjag



FULL LENGTH ARTICLE

1D and 3D inversion of VES data to outline a fresh water zone floating over saline water body at the northwestern coast of Egypt



Usama Massoud^{*}, Mamdouh Soliman, Ayman Taha, Ashraf Khozym, Hany Salah

National Research Institute of Astronomy and Geophysics (NRIAG), 11421 Helwan, Cairo, Egypt

Received 28 July 2015; revised 26 September 2015; accepted 2 November 2015

Available online 30 November 2015

KEYWORDS

VES data;
 1-D/3-D inversion;
 Seawater intrusion;
 Northwestern coast;
 Egypt

Abstract Seawater intrusion is a widespread environmental problem in the Egyptian coastal aquifers. It affects the groundwater used in domestic and agricultural activities along these coasts. In this study, resistivity survey in the form of Vertical Electrical Sounding (VES) was conducted at ZAWYET EL HAWALA cultivated site, northwest coast of Egypt to outline a freshwater zone overlies the main saltwater body, and to determine the most suitable location for drilling water well for irrigation purposes. The VES data were measured at 11 stations in the studied site. After processing, the data were inverted in 1-D and 3-D schemes and the final model was presented as resistivity slices with depth. The results indicate that the effect of saltwater intrusion was observed, as low resistivity values, at 7.5 m below ground surface (bgs) at the northern part of the study area (toward the Mediterranean Sea), and extends southward with increasing depth covering the whole area at about 30 m bgs. The fresh water zone shows a minimum thickness of less than 7.5 m at the northern side and a maximum thickness of about 20 m at the southern side of the area. The proper site for drilling water well tap and the freshwater zone is the location of VES6 or VES9 with a maximum well depth of about 20 m bgs. The water withdrawal from the proposed well should be controlled not to raise the main saline water table in the well site. The main sources of the freshwater zone are the rainfall and surface runoff descending from the southern tableland. Excess rainfall and surface runoff can be avoided from direct discharge to the sea by collecting them in man-made outlined trenches and re-using the stored water in irrigation during the dry seasons.

© 2015 Production and hosting by Elsevier B.V. on behalf of National Research Institute of Astronomy and Geophysics.

^{*} Corresponding author.

E-mail address: usaad2007@yahoo.com (U. Massoud).

Peer review under responsibility of National Research Institute of Astronomy and Geophysics.



Production and hosting by Elsevier

1. Introduction

Egypt is an arid zone with virtually 96% of its territory an uninhabited area. Although the Nile Valley and Delta are about 4% of the Egyptian land area, they are inhabited by about 80% of the Egyptian populations (Sayed, 2013). The overall growth of population and the rural–urban migration

flow in Egypt led to a tremendous growth of the main cities. Hoping to divert the people's movement away from these urban centers, the Egyptian Government has organized several programs to develop the coastal areas in order to enforce the national economy and to overcome the problem of population growth. These development programs have been already started along the Egyptian coasts in the form of new urban, industrial and agricultural projects. One of these programs was directed to the northwestern coast of Egypt, which embraces about 300 km of the Mediterranean coastline between Alexandria (east) and Matrouh (west). The landscape of this coast comprises two main features: the northern coastal plain and the southern tableland. The coastal plain has attracted many touristic projects with massive investments in the form of resorts, hotels, and touristic villages for recreation and swimming purposes (El-Sharnouby et al., 2011). In addition to the big projects, different activities are carried out by the local people residing along this coast including agriculture, grazing and agro-industries as picking olives, olive oil industry, drying fig, mint, and palm, handicraft of the palm leaves, etc.

The main problem encountered along this coastal area is the lack of water sources. Three possible sources are available at this area for water supplies needed for drinking, agriculture and other activities. The first water source is a pipeline carries the Nile water from Alexandria, follows the coastline and ends at Matrouh. It provides about 10,000 m³/day of drinking water which is insufficient but it is supplemented by the desalination units. The second source is the direct rainfall and surface flood water, where the precipitation rate is about 140 mm/year occurs mostly in winter time (El Bastawesy et al., 2008). The third one is the ground water infiltrated from the rainfall and surface runoff. This water can be stored naturally in the aquifers or artificially through the man-made cisterns (El-Raey, 1998). However, the groundwater aquifers along the northwestern coast are greatly affected by seawater invasion (e.g. Soliman et al., 2013; Khalil et al., 2013). So, all of the available sources for water supplies in the coastal areas are insufficient due to the reasons mentioned above.

The area of study is named ZAWYET ELHAWALA. It is located along Matrouh–Alexandria coastal road at about 25 km east of Matrouh city. This area is a cultivated land owned by individuals, measures about 1300 m × 1000 m (300 acre) and is bounded by latitudes 31° 11' 45" and 31° 12' 16" N, and longitudes 27° 27' 07" and 27° 27' 54" E as shown in Fig. 1.

This land site has been planted by olive and fig trees several years ago, where it was depending on seasonal rainfall and floods for irrigation. As the fig and olive trees are characterized by their capability to store water for long time, they were irrigated seasonally during the winter time and depend on the water stored in roots until giving their mature fruits in summer season. During the last few years and due to instability in the rainy winter, the area faced a scarcity in the rainfall which is the sole source for irrigation of this land. Accordingly, the trees started to dry due to the long time passed without irrigation. Then, it was vital to look for an alternative, even limited, water source to be used for irrigation during seasons with no rainfall. The groundwater can be considered as an alternative source for water supplies in this area especially it is located in the downstream of some drainage lines dissect the southern tableland. A great number of northward-flowing drainage lines (Wadis) dissect the elevated tableland, where the ground

surface is dipping northward as indicated by the elevation levels (Fig. 1), surface runoff is possible after heavy rains, and a considerable amount of water may percolate to deeper soil layers in the study area. The study area is not far from the Mediterranean Sea (about 1500 m). So, it is expected that the groundwater bodies are affected by the in-land saltwater intrusion.

The electrical resistivity method has been extensively used for mapping groundwater aquifers (Christensen and Sørensen, 1998), for investigation of aquifer vulnerability (Sørensen et al., 2005) and for freshwater/saline water studies (Khalil et al., 2013). So, this study was carried out to outline the freshwater zone, to trace the freshwater/saline water interface, and to determine the proper location for drilling new water well to be used for irrigation purposes in this cultivated-land area by 1-D and 3-D inversions of vertical electrical sounding (VES) data.

2. Geological setting

On the regional scale, the northwestern coast of Egypt comprises two geomorphic units: the tableland to the south and the coastal plain to the north between them a northward sloping piedmont zone (Shata, 1957; Hammad, 1972). The tableland is composed mainly of fissured limestone with a highly weathered top part. Besides, it is much undulated and locally covered by alluvial deposits and rock fragments. Outlets of the drainage lines, which pass to the coastal plain from high intake areas, usually break the bounding slopes. The coastal plain occupies the coastline of Mediterranean Sea, where it is represented by two elongated, foreshore and inland, ridges and two shallow depressions as shown in Fig. 2. The ridges are running parallel to the present shoreline, rising sometimes to more than 40 m, acting as watershed areas during rainy season, and attaining lower altitude toward the shoreline. The coastal ridges are missed or deformed at some locations as a result of local structures and/or erosion effect. In addition to the ridges, the coastal plain is occupied by other features such as sand dunes, sand beaches and marches.

The northwestern coast of Egypt is totally occupied by sedimentary rocks belonging to Quaternary and Tertiary (Fig. 3). Quaternary deposits are represented by the Holocene and Pleistocene sediments, while Tertiary deposits are represented by the Pliocene and Miocene sedimentary formations (Fig. 4). In the study area, the Pliocene deposits are absent and the Quaternary deposits rest uncomfortably over the Miocene deposits.

The Holocene deposits comprise two layers. The upper one consists of loose quartz sands mixed with carbonate grains and shell fragments. The lower layer is composed of alluvial deposits including calcareous loam sheets, friable mixture of clay, silt and sand particles containing organic material and shell fragments, uncomfortably rest over the Pleistocene deposits. The Holocene deposits are water-bearing where they are recharged from the rainfall, surface runoff and seepage from the main groundwater aquifers (Soliman et al., 2013). The Pleistocene deposits are detected in several localities along the northwestern coast. They are composed of oolitic limestone interbedded with thin bands of sand, sandstone and clay constituting elongated ridges in the coastal plain. In the study area, the Pleistocene deposits rest uncomfortably over the Middle Miocene deposits (Shaaban, 2004). The oolitic limestone represents

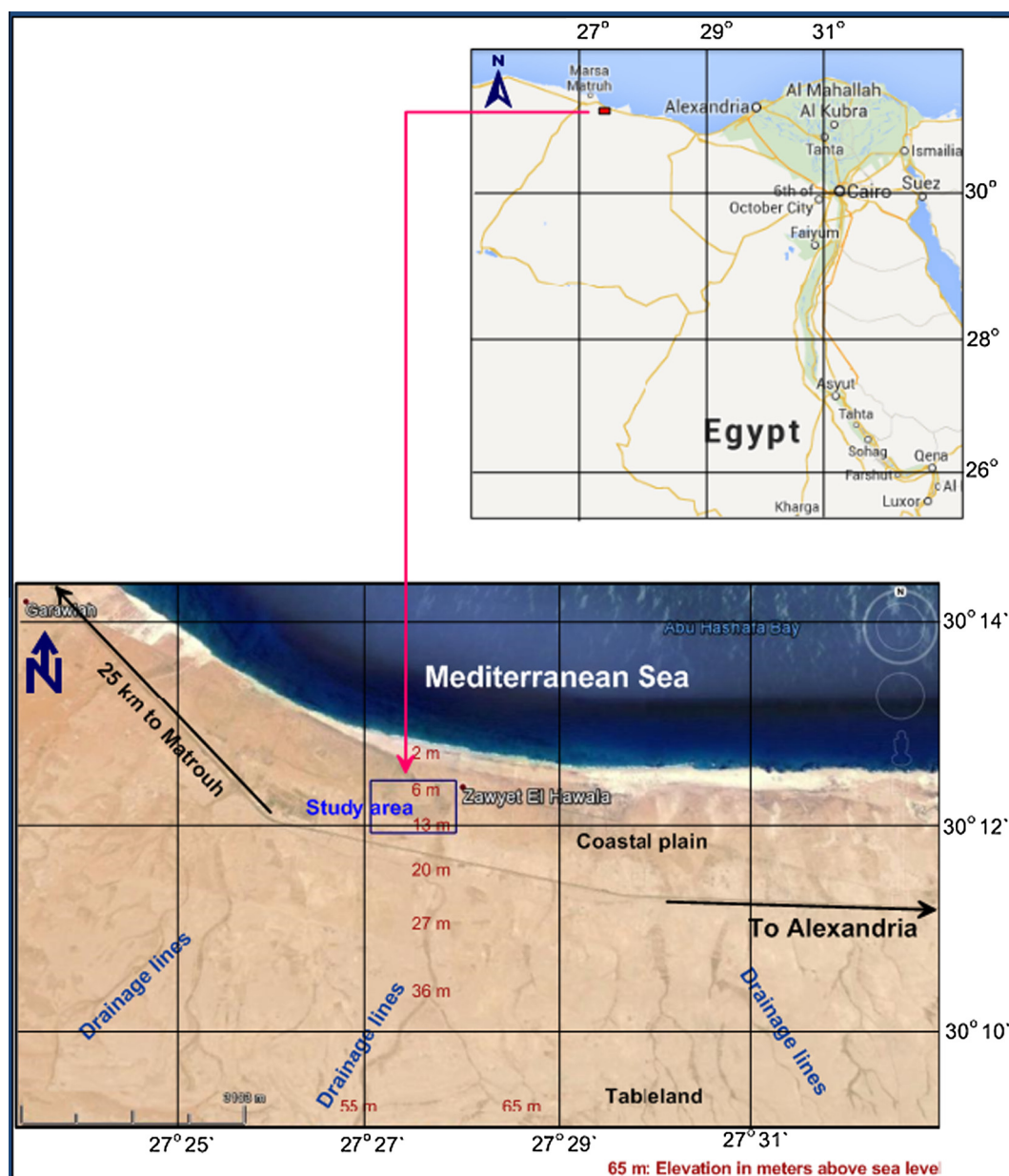


Figure 1 Location map of the study area.

the main groundwater aquifer in many locations along the northwestern coast. It is characterized by high primary porosity and existence of solution cavities that increase its capability to store large quantity of water. The groundwater quality of the oolitic limestone aquifer is changed vertically from freshwater at the top to saline at the base (El-Shazly, 1970). The Tertiary deposits are exposed at the southern tableland, where they are dissected by wadis and northward drainage lines. The Pliocene deposits consist of sand, clay, and marly limestone, and show limited exposures in the northwestern coast. In the study area, the Miocene deposits are represented by Marmarica Formation of Middle Miocene age which constitutes the major part of the southern tableland and consists of fractured limestone and dolomitic limestone intercalated with shale and marl (Yousif et al., 2013). The Miocene sediments represent the main deep groundwater aquifer in the northwestern coast,

where they are affected by a fracturing system plays an important role in recharging of this aquifer (Said, 1962; El-Shazly, 1970).

3. Hydrogeological regime

Several authors have studied the hydrogeology of the northwestern coast of Egypt (e.g. Abdel-Mogheeth et al., 1978; Sewidan, 1978; El Maghraby, 1997; El-Raey, 1998; El-Sharabi, 2000; Soliman, 2005 and others). They concluded that there are three (Holocene, Pleistocene and Middle Miocene) main aquifers in the northwestern coast including the study area. The Holocene aquifer consists of unconsolidated calcareous sand of high porosity which acts as a local reservoir for the direct rainfall and accumulated surface runoff at the coast. Pleistocene aquifer is

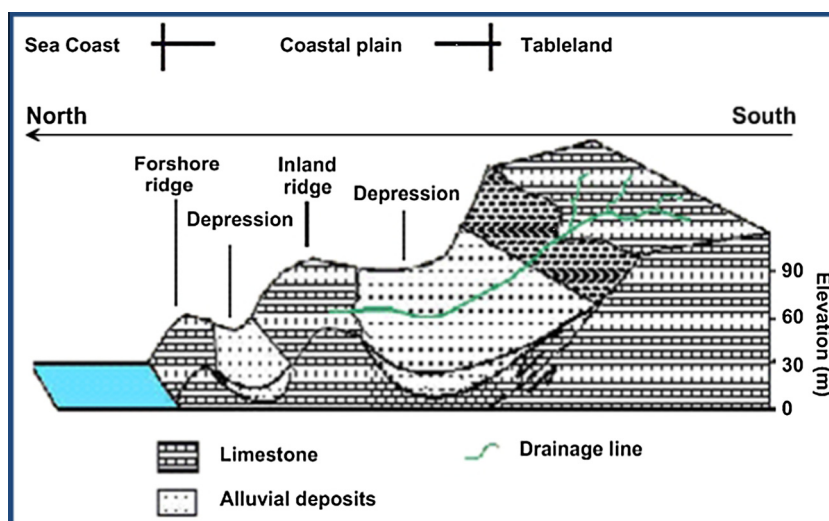


Figure 2 North-south graphical section showing landforms of the northwestern coast (Hammad, 1972).

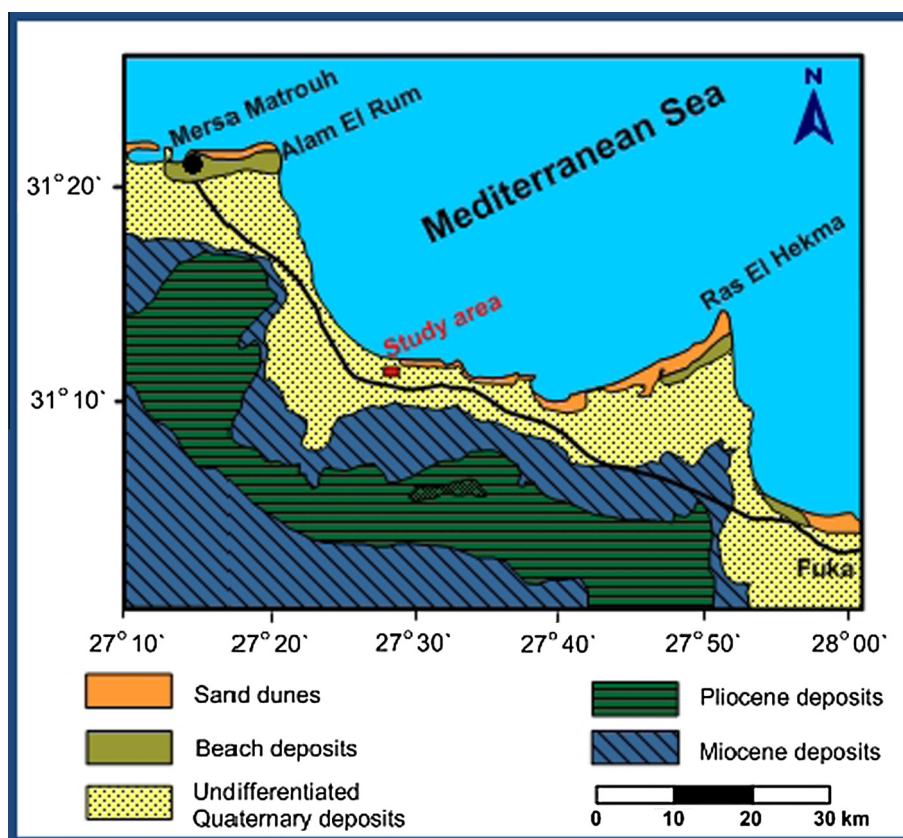


Figure 3 Geological map of the study area and its surroundings (CONOCO, 1986).

composed of oolitic limestone, and is considered as a main aquifer in the northwestern coastal zone. The water in this aquifer exists under free conditions and the main water table is almost determined by the inland seawater intrusion. The Middle Miocene aquifer (Marmarica Formation) is composed of limestone, dolomitic limestone intercalated with marl, clay and chalk.

4. Resistivity data

4.1. Data acquisition

In the study site, the VES data were measured at 11 points arranged in a grid-like pattern based on the available free spaces among the trees. The spacing between the measuring








Age			Lithology & Description	Thickness	Hydrology	
Period	Epoch					
Quaternary	Holocene	Recent deposits		Loose yellow to brown quartz sand mixed with carbonate grains and shell fragments	< 3 m	-----
		Alluvial deposits		Plae brown calcareous loam mixed with sands, shell fragments and organic material	~ 10 m	-----
	Pleistocene			Plae brown detertal oolitic limestone	~ 60 m	Main shallow aquifer (unconfined)
				Very hard limeatone composed of shell aggregates and gravel cemented by lime	~ 40 m	Partially saturated (limited)
Tertiary	Pliocene			Plae brown clay and fine sands with moderately hard limestone at top	< 70 m	Secondary aquifer
	Miocene	Middle		White to plae yellow fossiliferous limestone interbedded with marl and clays	More than 1000 m	Main deep aquifer (wide)
		Lower		Fine to coarse grained yellow sandstone interbedded with shale and silt		Main deep aquifer (artesian)

Figure 4 General litho-stratigraphic column of the study area (Hilmy et al., 1978; El-Sharabi, 2000).

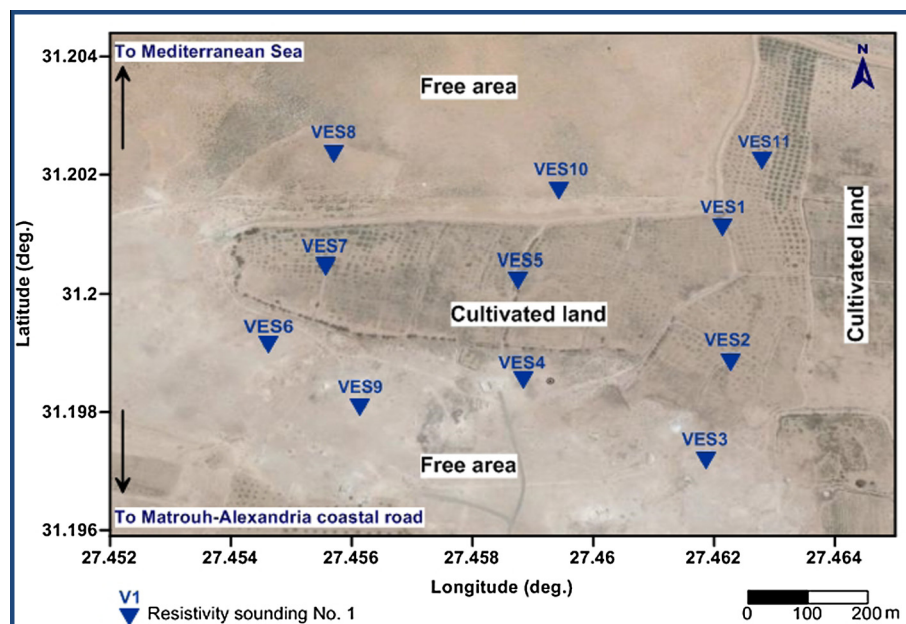


Figure 5 Distribution of the measuring points of VES data in the investigated site.

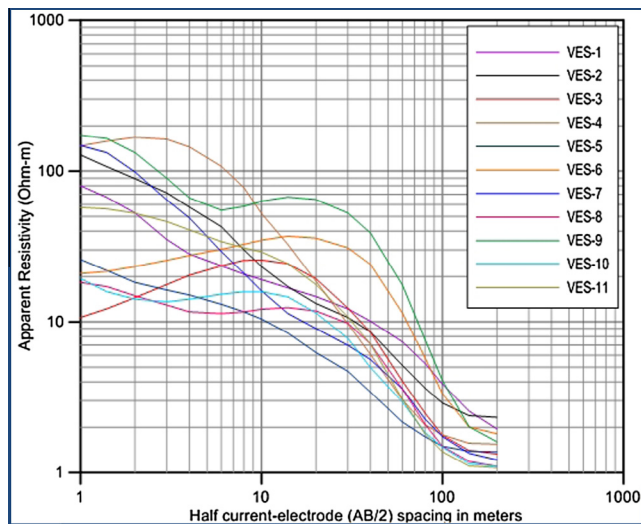


Figure 6 Sounding curves obtained from the measured resistivity data at the study area.

points was ranging from 200 to 300 m (Fig. 5). Resistivity data were measured by SYSCAL-R2 resistivity meter (IRIS Instruments, 1998). It is a high-power, fully automated resistivity meter for DC electrical survey. The measuring process was optimized to provide the best possible accuracy in the field conditions. The field survey was carried out by applying the standard Schlumberger electrode array with current-electrodes (AB) spacing varying logarithmically from 2 to 400 m. The spreading direction of the array was unified in the north-south direction for the measured points. The short spacing between the measuring points and the unified spreading direction made the measured data proper for the 3-D inversion process.

4.2. Sounding curves

The apparent resistivity values (ρ_a) are plotted against the half-current electrode spacing on a log-log paper to give the

so-called resistivity sounding curve. Sounding curves for all measured data are shown in Fig. 6. It is worth to mention that the field measurements were initiated by increasing the half-current electrode spacing (AB/2) to more than 200 m. However, no change in the measured resistivity values could be obtained beyond AB/2 = 200 m. This indicates that the electric current maybe entrapped within a very-low resistivity layer and does not go deeper especially the apparent resistivity values at AB/2 = 200 m were concentrated around 2 Ohm m as shown in Fig. 6. This highly conductive layer was reported as a water-bearing layer fully saturated with saline water due to sea water invasion to the coastal aquifers as the aquifers are in direct contact with the Mediterranean Sea (El-Sharabi, 2000; Soliman, 2005; Yousif et al., 2013).

Inspection of the sounding curves (Fig. 6) reveals that the apparent resistivity values in the first logarithmic cycle (AB/2 = 1–10 m) show different behaviors and different starting values based on the surface weathering and lithological heterogeneity of the near surface medium. In the second cycle (AB/2 = 10–100 m), the measured values have shown moderate resistivity values (10–70 Ohm-m) at AB/2 = 10 m and the values were descended with increasing AB/2 spacing. Ongoing downward (AB/2 > 100 m), the measured resistivity values were concentrated around 2 Ohm-m for all the measuring stations.

4.3. 1-D inversion

The measured resistivity data were first processed to remove the erroneous values straying from the general trend. Then, the smoothed data were inverted in terms of 1-D multi-layer earth models. An initial model was obtained from the geological and hydrogeological information available for the study area. Then, a semi-automatic iterative approach was used to refine the initial model. The computer program (IPI2Win-1D, 2000) was used to calculate the final resistivity model. The root mean square (rms) errors between the observed and calculated resistivity values ranged from 1.04% to 1.97%. Fig. 7 shows two examples of the models obtained at the measuring points VES4 and VES10, where the model response

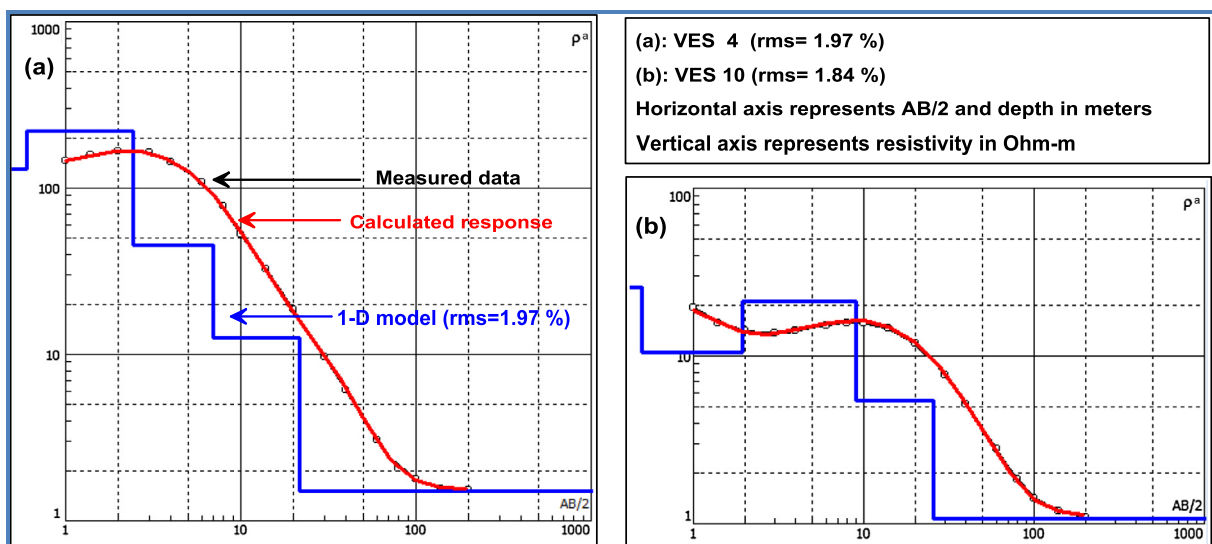


Figure 7 1-D models obtained from resistivity data inversion at VES4 and VES10.

(red line) exhibits a good fit with the measured data (open circles).

Inspection of the 1-D models revealed that the investigated subsurface comprises 4–5 geoelectrical layers with a maximum attained depth of less than 30 m. The detected layers beneath all measuring points show a wide range of resistivity values varying from 5.5 to 220 Ohm m except for the last (deepest) layer which shows very low resistivity (around 2 Ohm m) underneath all sounding points. The markedly low resistivity values shown by the last detected layer in the study area could be attributed to the effect of seawater invasion, where the main water table is almost determined by the inland seawater intrusion (Yousif et al., 2013).

Investigation of the resistivity sounding curves (Fig. 6) and the true resistivity values obtained by 1-D inversion (examples in Fig. 7) revealed that the sounding curves show different behaviors and the true values show big variation from site to site in the first and second log cycles ($AB/2 = 1\text{--}10$ m and $10\text{--}100$ m). This may be attributed to lithological variation and different levels of seawater effects. To better understand the lateral and vertical distribution of resistivity as well as the seawater intrusion pattern in the shallow subsurface, the smoothed sounding data have undergone a 3-D inversion process.

4.4. 3-D inversion

The greatest limitation of the conventional 1-D resistivity sounding method is that it does not incorporate lateral changes in the layer resistivity. Such changes are probably the rule rather than the exception, where the ideal 1-D layered earth is rarely found in practice. A more accurate model of the subsurface is 2-D, where the resistivity changes in the vertical direction, as well as in the horizontal direction along the survey line, assuming that resistivity does not change perpendicular to the survey line. If this is not the case, a 3-D resistivity survey and inversion should be much more accurate. With advent of the powerful measuring systems and the high computing power, new 2-D and 3-D surveys and inversion codes have been developed (e.g. Loke and Barker, 1996; Günther, 2004; Marescot et al., 2005). Moreover, some authors have devoted their research work to the 2-D and 3-D inversion of Schlumberger sounding data (Tripp et al., 1984; Tong and Yang, 1990; Uchida, 1991; Santos and Sultan, 2008).

4.5. 3-D inversion scheme

In the present study, we used the code developed by Santos and Sultan (2008). The scheme is based on that one proposed by Sasaki (1994, 2001). The problem is linearized as follows:

$$J\Delta p = \Delta d \quad (1)$$

where Δp is the vector containing the corrections to the model parameters p , $\Delta d = y^c - y^{ob}$ is the vector of differences between the model responses and the measured data, and J is the derivative matrix (Jacobian) containing the derivatives of the model responses with respect to the model parameters ($J_{ij} = \partial y_i^c / \partial p_j$). The code allows the exact calculation of the derivative matrix, using the reciprocity principle, or its estimation using the algorithm presented by Loke and Barker (1996) and assuming that each block is embedded in a homogeneous

half-space. In this case the Jacobian value is subsequently updated by using Broyden's method (1965). The minimization of an appropriate objective function allows the estimation of the corrections to the model parameters in each iteration.

The used code allows the user to choose between two different objective functions to be minimized.

$$\text{The first one is : } Q = \|W_d(\Delta d - J\Delta p)\|^2 + \lambda \|C\Delta p\|^2 \quad (2)$$

Minimization of this function yields the normal equations (see details in Sasaki, 1994) as follows:

$$(J^T W_d^T W_d J + \lambda C^T C) \Delta p = J^T W_d^T W_d \Delta d \quad (2.1)$$

where W_d is a diagonal matrix consisting of the reciprocal of the data standard deviations and C is the roughness operator.

The second objective function (Sasaki 2001) is as follows:

$$Q = \|W_d(\Delta d - J\Delta p)\|^2 + \lambda [\|C\Delta p\|^2 + \alpha \|W_p(p_b - p)\|^2] \quad (3)$$

Minimizing of this function produces the system of equations as follows:

$$\begin{aligned} (J^T W_d^T W_d J + \lambda C^T C + \lambda \alpha W_p^T W_p) \Delta p \\ = J^T W_d^T W_d \Delta d - \lambda C^T C p + \lambda \alpha W_p^T W_p (p_b - p) \end{aligned} \quad (3.1)$$

where W_p is a diagonal matrix used to control the closeness of the parameters to an initial model, expressed in the vector p_b , and C is the roughness operator. The parameter λ is a Lagrange multiplier, and α is used to control the balance between the model smoothness and the closeness to the initial model.

Normal Eqs. (2.1) and (3.1) were solved by means of a conjugate gradient method. The model parameters were then updated by adding the vector Δp and the iteration procedure continued until the misfit is reduced to an acceptable level. The rms misfit is given by Eq. (4), where N is the number of data points.

$$\text{rms \%} = \frac{100}{N} \sum_{i=1}^N \sqrt{\left(\frac{y_i^c - y_i^{ob}}{y_i^{ob}} \right)^2} \quad (4)$$

Sensitivity volume (Φ) of Schlumberger array is defined by the following:

$$\Phi = (\rho_j / \rho_i) \partial \rho_i / \partial \rho_j \quad (5)$$

where ρ_j is the resistivity of the j th model block and ρ_i is the apparent resistivity calculated at the i th observation site. The function Φ reflects the change of the apparent resistivity at the observation site due to the change in resistivity of a specific model block. Therefore, it is possible to evaluate the influence of the different model blocks on the measurements. ‘‘Sensitivity volume’’ of the Schlumberger array is smaller than that one defined for the dipole–dipole array. So, the multi-dimensional investigation by using VES data needs a close measurement sites.

In this study, the VES data were inverted by using 3-D algorithm based on finite element and regularization method developed by Santos and Sultan (2008). The 3-D inversion process was applied to a specific part ($AB/2 = 1\text{--}60$ m) of the sounding data because: (1) the selected part is expected to cover the shallow subsurface medium that involves the freshwater zone, (2) the effect of seawater intrusion was expected to appear at a depth level less than the corresponding depth of $AB/2 = 60$ m as observed in the sounding curves (Fig. 6),

and (3) if we used the entire sounding curve until $AB/2 = 200$ m, the calculated response of the input model cannot fit well both the high resistivity values at the shallow subsurface and the very low values at the deeper medium.

In the 3-D inversion, the subsurface medium was divided into $25 \times 20 \times 12$ (in X , Y , Z directions, respectively) blocks

with unknown resistivity, and the mesh used for forward calculation was automatically adapted for each sounding. The root mean square (rms) difference between the observed and calculated resistivities was used to determine the appropriateness of the model. Generally, the fitting is acceptable even though there are existed slight misfits at short electrode spacings which

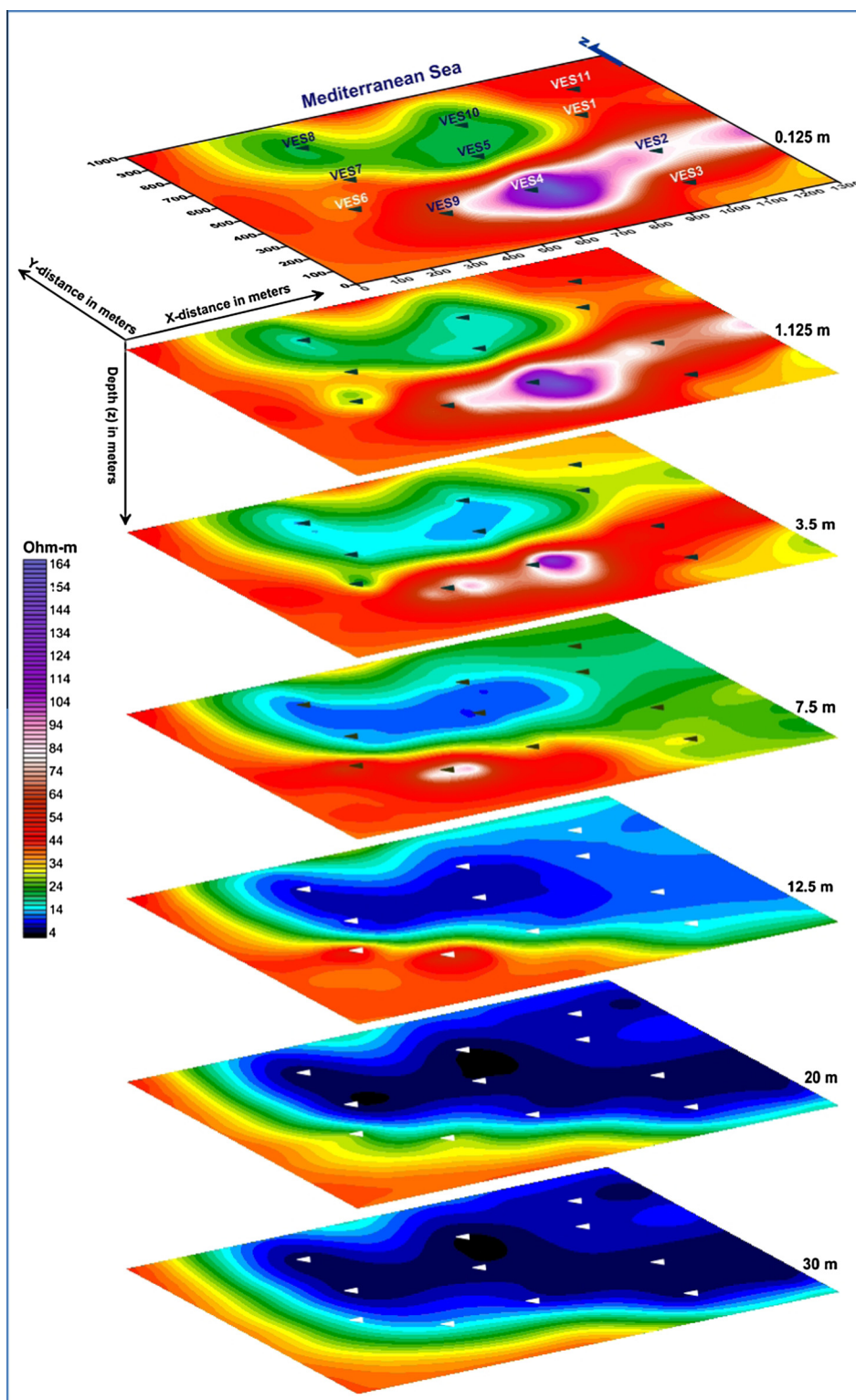


Figure 8 3-D resistivity model obtained from VES data inversion. Locations and numbers of the soundings are shown on the uppermost slice.

may be due to surface conditions. The rms value was 7.2% after 10 iterations, where no further enhancement in the fitting was obtained beyond the sixth iteration.

5. Results

The inversion results were presented as horizontal slices of the resistivity model as a function of depth (Fig. 8).

6. Discussion

Vertically, the model shows a general decreasing of resistivity with depth for all soundings except for locations of VES6 and VES9 which show an initial downward increasing of resistivity (Fig. 8) until 7.5 m below ground surface (bgs) and started to decrease with depth. The lateral variation of resistivity values from site to site in the study area was controlled by the elevation of each site above sea level. Accordingly, the sites with low elevations show low resistivity values than the highly elevated sites because the low-elevation sites are affected earlier by the sea water invasion than the highly elevated locations.

In the study area, the ground surface shows a general northward slope. So, the obtained resistivity values are low at the northern soundings (VES5, VES7, VES8, and VES10) as these points are located at low land area near the Mediterranean Sea. On the other side, high resistivity values were obtained at the southern soundings which occupy elevated locations toward the feeding drainage lines descending from the southern tableland.

In light of the available geological and hydrogeological information, the upper part of the investigated section (0–10 m depth) represents the Holocene deposits and the lower part (below 10 m depth) are the Pleistocene deposits. The low resistivity values observed in the investigated section could be interpreted as zones containing saline water and the high resistivity values could indicate freshwater-containing zones. The effect of sea water was firstly appeared, in the form of low resistivity, at 7.5 m bgs at the low elevation sites (VES5, VES7, VES8, and VES10). Ongoing downward, the effect of sea water invasion was extended southward to include the locations of VES1, VES2, VES3, VES4 and VES11. The locations of VES6 and VES9 kept high resistivity values until 20 m depth. Beyond 20 m bgs, the whole study area was invaded by saline water as shown in the lowermost (30 m) slice in Fig. 8.

The regional water table in the study area is determined by the sea water level which has appeared at shallower depth in the northern side and deepens southward. So, the thickness of the freshwater zone is less than 7.5 m (the first appearance of sea water effect) in the north and is increased to about 20 m in the southern part of the study area. The possibility of obtaining a reasonable quantity of water from this freshwater zone is increased with moving southward. The most proper sites for drilling water wells in the study area are the locations of VES6 and VES9 with a maximum well depth of 20 m bgs.

The main feeding sources of the freshwater lens are the direct rainfall and surface runoff from the drainage lines descending from the southern highly elevated area. Water withdrawal from the proposed well should be limited because over pumping of this well may lead to rising of the main saline water table in the well site. No confining layers are existed in the Holocene sediments of the coastal plain. So, excessive

rainfall and surface runoff are discharged directly to the sea. Then, another possibility for obtaining water can be done by excavation of man-made outlined trenches to trap and store excessive water during the heavy rain season and reuse this water for irrigation purposes in dry season.

7. Conclusion

1-D and 3-D inversions of VES data were successfully used to outline the shallow freshwater zone at Zawyet El Hawala site, northwestern coast of Egypt, and to determine the lateral and vertical extensions of this freshwater body. The freshwater zone shows a minimum thickness of about 7 m at the northern side of the study area toward Mediterranean Sea and a maximum thickness of about 20 m at the southern part. The effect of sea water, in the form of low resistivity structure, was firstly appeared at 7.5 m bgs in the northern part and it was extended southward with increasing depth until it covered the whole area at about 30 m bgs. The most proper sites for drilling water well are the locations of VES6 or VES9 as they show relatively high resistivity values (low salinity) until 20 m bgs. The pumping from the proposed well should be limited not to raise the saline water table at the well site. Excessive rainfall and surface runoff during the heavy rain season can be collected in man-made outlined trenches to be used for irrigation purposes during the dry season.

Acknowledgments

The authors express their deep thanks to the members of the geoelectric and geothermic Lab., National Research Institute of Astronomy and Geophysics (NRIAG) due to their kind help during the field work.

References

- Abdel-Mogheeth, S.M., Taha, A.A., Hammad, F.A., 1978. Hydrogeological Studies on the Tertiary and Quaternary Aquifers Along the Coastal Zone of Egypt and Libya. Water Research Institute, Cairo, Internal Report.
- Broyden, 1965. A class of methods for solving nonlinear simultaneous equations. *Math. Comput.* 19, 577–593.
- Christensen, N.B., Sørensen, K.I., 1998. Surface and borehole electric and electromagnetic methods for hydrogeological investigations. *Eur. J. Environ. Eng. Geophys.* 3, 75–90.
- CONOCO, 1986. Geological Map of Egypt, Scale 1: 500,000 GPC, Sheet No. NH35NE.
- El Bastawesy, M.A., Ali, R.R., Nasr, A.H., 2008. The use of remote sensing and GIS for catchments delineation in Northwestern Coast of Egypt: an assessment of water resources and soil potential. *Egypt J. Remote Sens. Space Sci.* 11, 3–16.
- El Maghraby, M., 1997. Geophysical, Hydrogeological and Remote Sensing Studies on the Effect of Sea Level Fluctuation on the Groundwater Reservoir between Alexandria and El Daba'a, Egypt. Ph.D. Thesis, Fac Sci Alex Univ, p. 357.
- El-Raey, M., 1998. Framework of Integrated Coastal Area Management of the Fuka-Matrouh Area, Egypt: PAP/RAC-37-1995.
- El-Sharabi, E.S., 2000. Hydrogeological, Geomorphological and Geoenvironmental Implications for Future Sustainable Development of the Northwestern Coastal Zone of Egypt. Ph. D. Thesis, Mansoura University, p. 346.
- El-Sharnouby, B., Soliman, A., El-Nagar, M., El-Shahat, M., 2011. Study of environmental friendly porous suspended breakwater for the Egyptian Western North Coast. *Ocean Eng.* 48, 47–58.

- El-Shazly, M.M., 1970. Contribution to the geochemistry of the groundwater in Mersa Matruh area (western Mediterranean coastal zone, Egypt). *Bull. Inst. Desert, Cairo* 20 (2), 289–299.
- Günther, T., 2004. Inversion Methods and Resolution Analysis for the 2D/3D Reconstruction of Resistivity Structures from DC Measurements. Dr. sRer. Nat. thesis. Fac. Geowissenschaften, Geotechnik und Bergbau der Technischen Univ. Bergakademie Freiberg, Germany.
- Hammad, F.A., 1972. The Geology of the Soil and Water Resources in the Area Between Ras El-Hekma and Ras Alam El-Rum (Western Mediterranean Littoral Zone, Egypt). Ph.D. Thesis, Fac. Sci., Cairo Univ., Cairo.
- Hilmy, M., El Shazly, M., Korany, E., 1978. Lithostratigraphy and petrology of the Miocene and post-Miocene sediments in Burg El Arab-El Daba'a area. *Desert Inst. Bull. ARE* 28 (1), 1–24.
- IPI2Win-1D Program, 2000. Programs set for 1D VES data Interpretation, Dept. of Geophysics, Geological faculty, Moscow University, Russia.
- IRIS-INSTRUMENTS, 1998. User's Manual of Syscal Junior-Syscal R2, Multi-Electrode System, Orleans Cedex, p. 98.
- Khalil, M.A., Abbas, A.M., Santos, F., Massoud, U., Salah, H., 2013. Application of VES and TDEM techniques to investigate sea water intrusion in Sidi Abdel Rahman area, northwestern coast of Egypt. *Arab. J. Geosci.* 6, 3093–3101.
- Loke, M.H., Barker, R.D., 1996. Rapid least-squares inversion of apparent resistivity pseudo sections by a quasi-Newton method. *Geophys. Prospect.* 44, 131–152.
- Marescot, L., Palma Lopes, S., Rigobert, S., Lagabrielle, R., Chapellier, D., 2005. Nonlinear resistivity inversion on three-dimensional structures using the finite element method. *Geophys. Res. Abstracts* 7, 09948.
- Said, R., 1962. The Geology of Egypt. Elsevier Publisher, Amsterdam and New York.
- Santos, F.A.M., Sultan, A.S., 2008. On the 3-D inversion of vertical electrical soundings: application to the South Ismailia area – Cairo Desert Road, Cairo Egypt. *J. Appl. Geophys.* 65, 97–110.
- Sasaki, Y., 1994. 3-D resistivity inversion using the finite element method. *Geophysics* 59 (11), 1839–1848.
- Sasaki, Y., 2001. Full 3-D inversion of electromagnetic data on PC. *J. Appl. Geophys.* 46, 45–54.
- Sayed, A.S.A., 2013. Evaluation of the Land Resources for Agricultural Development – Case Study: El Hammam canal and its extension, NW coast of Egypt. Ph. D. Dissertation, Department Geowissenschaften der Universität Hamburg, p. 241.
- Sewidan, A.S., 1978. Water Budget Analysis for the Northwestern Coastal Zone. Ph.D. Thesis, Fac. Sci. Cairo Univ., p. 179.
- Shaaban, F.A., 2004. Geophysical evaluation of the groundwater potentiality, southeast Matrouh area, Egypt. *NRIAG J. Geophys.*, 243–266, Special Issue
- Shata, A., 1957. Geology and geomorphology of the Wadi El-Kharruba area, Western Desert, Mediterranean littoral, Matrouh District, Egypt. *Bull. Inst. Desert D' Egypt* (10), 91–120.
- Soliman, M.M., Massoud, U., Mesbah, H., Ragab, E., 2013. Mapping of sea water/freshwater interface at the northwestern coast of Egypt by 2-D resistivity imaging and transient electromagnetic soundings. Society of Exploration Geophysicists, SEG Annual Meeting, 22–27 September 2013, Houston, Texas, pp. 1955–1960.
- Soliman, M.M., 2005. Environmental and Geophysical Assessment of the Ground and Subsurface Water Resources of Ras El-Hekma Area, Northwestern Coast of Egypt. Ph. D. Thesis, Faculty of Science, Ain Shams University, Cairo, Egypt. p. 148.
- Sørensen, K.I., Auken, E., Christensen, N.B., Pellerin, L., 2005. An integrated approach for hydrogeophysical investigations: new technologies and a case history. *Near-Surf. Geophys.* 2, 585–603.
- Tong, L.T., Yang, C.H., 1990. Incorporation of topography into two-dimensional resistivity inversion. *Geophysics* 55, 354–361.
- Tripp, A.C., Hohmann, G.W., Swift, C.M., 1984. Two-dimensional resistivity inversion. *Geophysics* 49, 1708–1717.
- Uchida, T., 1991. Two-dimensional resistivity inversion for Schlumberger sounding. *Geophys. Explor. Jpn. (Butsuri Tansa)* 44 (1), 1–17.
- Yousif, M., El Abd, E., Baraka, A., 2013. Assessment of water resources in some drainage basins, northwestern coast, Egypt. *Appl. Water Sci.* 3, 439–452.